Computation of Pressure Distribution Using PIV Velocity Data

R. Gurka[(1)], A. Liberzon[(1)], D. Hefetz[(2)], D. Rubinstein[(1)], U. Shavit[(1)]*
[(1)] Agricultural Engineering, Technion, Haifa 32000, Israel (aguri@tx.technion.ac.il)
[(2)] Biomedical Engineering, Technion, Haifa 32000, Israel

Abstract Particle image velocimetry (PIV) can be used for pressure assessment. This non intrusive measurement method provide a high spatial resolution which is unavailable when using pressure transducers. The velocity vector information was used to solve inversely the Navier-Stokes equation to provide the pressure gradient needed for the Neumann boundary condition. Then the velocity data was used again to solve the pressure Poisson equation. Two flow problems were tested, water flow in a pipe with a constriction and an impinging air jet. The constriction flow was chosen to represent laminar flow problem where pressure is changing significantly. Results were compared with an inviscid solution and the effect of spatial resolution was examined. The impinging air jet was chosen to represent a turbulent flow problem. The pressure distribution on the impingement plate was compared with reported data from the literature and some aspects of time averaging were discussed.

1 Introduction

Particle Image Velocimetry (PIV) generates instantaneous velocity maps in a two dimensional cross section of flow problems. The spatial resolution and the accuracy of the measurement, if performed adequately, are considered to be high. The measured velocity can then be used for a wide range of post processing calculations, including velocity magnitude and direction, velocity gradient, viscous shear, stream function, vorticity, and others. Mean and fluctuating components can be calculated based on multiple realizations to represent the statistical parameters of unstable and turbulent flows. The pressure field in both laminar and turbulent flows is useful when forces are to calculated, when comparison with pressure gauging is required, and when better understanding of the flow problem is desired. Pressure gauges used for pressure measurement are expansive, large in their size, and require an actual contact with the fluid. When the measurement is performed intrusively the flow and pressure are affected by the procedure itself (e.g. while using a catheter for coronary procedures). It was suggested, therefore, to avoid such difficulties by computing the pressure field from the velocity data generated by the non intrusive particle image velocimetry method. In the current study we present calculation results of pressure fields based on the instantaneous velocity fields obtained by particle image velocimetry.

The calculation of the pressure field is determined by using the pressure Poisson equation which is derived by applying the divergence operator on the incompressible Newtonian Navier-Stockes equations,

$$\nabla^2 P = -\rho \nabla \cdot \{V \cdot \nabla V\}, \qquad \text{in} \quad \Omega \tag{1}$$

where P is the piazometric pressure, V is the velocity vector, and ρ is density. The representation of the two dimensional form of Eq. 1 in Cartesian coordinates is,

$$\nabla^2 P = -\rho \left\{ \left(\frac{\partial u}{\partial x}\right)^2 + 2\left(\frac{\partial u}{\partial y}\frac{\partial v}{\partial x}\right) + \left(\frac{\partial v}{\partial y}\right)^2 \right\} \tag{1a}$$

where u and v are the x and y components of V. The right hand side of Eq. 1 can be directly calculated from the velocity vector field generated by the PIV system.

Gresho and Sani (1987) have pointed out that the physical boundary conditions are to be derived from the conservation of momentum, namely the Navier Stokes equations. The correct boundary conditions for incompressible flow are, therefore, the Neumann boundary conditions rather than the Dirchelet conditions. Similar to the right hand side of the Poisson equation (Eq. 1), particle image velocimetry can be used to provide the required boundary pressure conditions by applying the Navier Stokes equations on the boundary, Γ, as follows,

$$\nabla P = -\rho\{\partial V/\partial t + V \cdot \nabla V\} + \mu \nabla^2 V \qquad (2)$$

where μ is the dynamic viscosity and t is time. When either steady laminar flow or steady mean turbulent flow are to be analyzed, the time derivative, $\partial V/\partial t$, is zero and the PIV data can be used to compute the $\rho\{V \cdot \nabla V\}$ and $\mu \nabla^2 V$ terms.

When turbulent flows are of interest, the Reynolds stress term is added to both Eqs. 1 and 2. The Neumann boundary conditions are obtained by solving the time average turbulent equations and the turbulent Poisson equation is hence,

$$\nabla^2 P = -\rho \nabla \cdot \{V \cdot \nabla V\} + \nabla \cdot \partial/\partial x_j (\overline{u_i' u_j'}) \qquad (3)$$

index notation was used such that $i, j = 1,2,3$ and u_i and x_i represent the velocity and location. Here V denotes the time averaged velocity vector. The Cartesian representation of $\nabla \cdot \partial/\partial x_j (\overline{u_i' u_j'})$ is,

$$\frac{\partial^2}{\partial x^2}(\overline{u'^2}) + 2\frac{\partial^2}{\partial x \partial y}(\overline{u'v'}) + \frac{\partial^2}{\partial y^2}(\overline{v'^2}) \qquad (4)$$

The pressure field calculation was tested for two flow problems; water flow in a pipe with a constriction and an impinging air jet. The constriction flow was chosen to represent laminar flow problem where pressure is changing significantly. Results were compared with an inviscid solution and the effect of spatial resolution was examined. The impinging air jet was chosen to represent a turbulent flow problem. The pressure distribution on the impingement plate was compared with reported data from the literature and some aspects of time averaging were discussed.

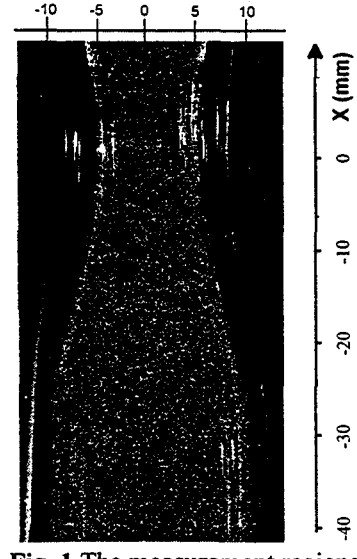

Fig. 1 The measurement regions.

2 Experimental

Constriction Flow A constant distilled water flow rate of 360 ml/min was circulated through a 20mm inner diameter glass tube with a 10mm inner diameter constriction. A 5μm Polyamid seeding particles (PSP-5, Dantec) solution was added to the distilled water, resulting in a concentration of 116

mg/l. A 160mJ per pulse Nd:YAG double laser system (Quantel), a cross correlation 1Kx1K CCD camera (Kodak, MEGAPLUS ES 1.0), an image acquisition system (OFS), and a home made analysis software was used for the particle image velocimetry. Mass flow rate was measured using a Coriolis acceleration flow meter (Micro-Motion). Water was circulated using a centrifugal pump and a constant head container to maintain a steady flow rate. Fully developed flow was achieved using an entry length of 21 diameters. The tube orientation was vertical and flow direction was upwards to avoid accumulation of air bubbles and sedimentation. Fig. 1 shows the glass tube.

The velocity vector field was generated by cross correlation within the two rectangular frames shown in Fig. 1. Calibration resulted in a micron to pixel ratio of 14.347 μm/pixel. Interrogation areas of 32x32 pixels (459.1μm x 459.1μm) and 64x64 pixels (918.2μm x 918.2μm) were used. The effect of measurement resolution was tested by repeating the PIV analysis every 4, 8, 16, 32, and 64 pixels (57.4, 114.8, 229.6, 459.1, and 918.2 μm). Results showed that vector validation and filtering was unnecessary. Filters such as signal to noise ratio and a local kernel comparison resulted in zero rejection. Forty realizations of the instantaneous velocity fields were obtained and averaged for each experiment.

Impinging air jet

The experimental setup consists of an air supply system, an aerosol generator, a mixing chamber and a convergence section, and a round smooth glass tube (length 300 mm, inner diameter 29.5 mm). A round flat plate (200 mm in diameter) was installed perpendicular to the flow, 1, 3, and 5 tube diameters downstream from the tube exit. A flow rate of $6.83e^{-4}$ m^3/s was used to meet the flow conditions of Peper et. al (1997) and was measured using a Micro-Motion coriolis based flow meter.

Propylene-glycol particles were generated by a Laskin aerosol generator resulting in an average diameter of 0.75 mμ (Echols and Young, 1963). A choice of 32x32 pixels square interrogation areas, a 57.8 mμ / pixel ratio, and repeating the PIV analysis every 16 pixels resulted in 3906 vectors in a field of 57.3 mm by 58.3 mm. For each distance between the tube exit and the plate ($1d_i$, $3d_i$, and $5d_i$, with d_i representing the nozzle diameter), 130 realizations of the instantaneous velocity fields were measured. Vector validation was obtained by a signal to noise filter and a local kernel comparison filter resulting in an average rejection rate of approximately 5%. One such velocity map is shown in Fig. 2.

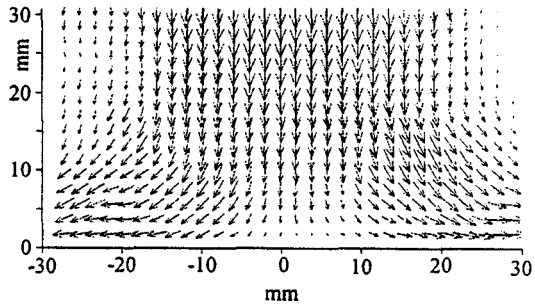

Fig. 2 An impinging jet velocity vector map.

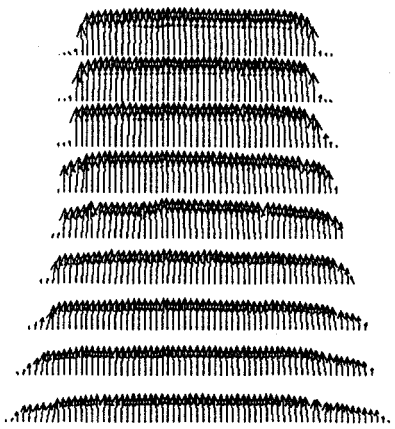

Fig. 3 A tube velocity vector map.

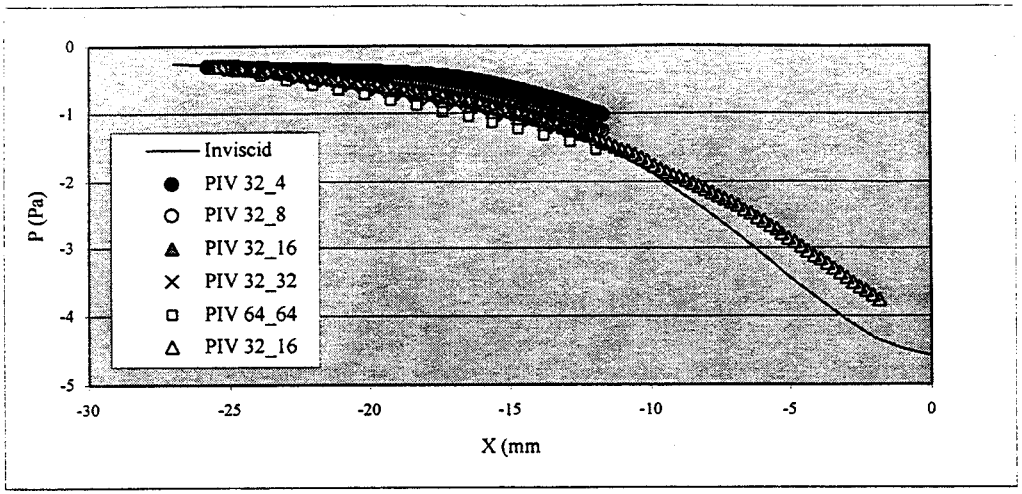

Fig. 4 Pressure profiles in the converging section of the tube. The curves in the first frame were obtained using a range of spatial resolution. The legend is consist of 2 numbers the first indicates the interrogation size and the second describes the vector spacing.

3 Results and Discussion

Constriction Flow Fig. 3 shows an instantaneous vector field in the converging section of the tube constriction. As the cross sectional area decreases, the axial velocity increases and the profile becomes less parabolic and more uniform. Although the lateral component is small its contribution to the pressure calculation was significant. As expected, the lateral component points towards the tube center line with a maximum near the region where converging slope is the largest. Fig. 4 shows that the pressure result is sensitive to the spatial resolution. High resolution (interrogation area of 32 pixels and spatial resolution of 4 pixels) generates a curve with a changing slope but is over predicting the pressure. Low resolution (interrogation area of 64 pixels and spatial resolution of 64 pixels) generates a curve with an almost constant slope and an under prediction of the pressure. The resolution which was chosen to be used for the analysis of the second frame ($x = -15 \div 0\,mm$) was of 16 pixels.

The impinging jet Prior to calculating the pressure of the impinging turbulent flow, a stagnation potential flow was used to test the pressure calculation procedure. This procedure starts by using the velocity components, u and v, and solving inversely the Navier-Stokes equations (Eq. 2) in order to provide the Neumann boundary conditions, ∇p on Γ. The velocity components, $u = -Cx$ and $v = Cy$ are determined by using the potential flow stream function, $\psi = Cxy$. The pressure gradient components, derived by the Navier-Stokes (Euler) equations, are $\partial p/\partial x = -\rho C^2 x$ and $\partial p/\partial y = -\rho C^2 y$. Hence, the boundary condition at y=0 is $\partial p/\partial y = 0$, the boundary conditions at the side boundaries are $\partial p/\partial x = \pm \rho C^2 L$, and the boundary condition at $y = y_L$ is a Dirichlet type, $p(x, y_L)$ (Corcos 1963) determined by the potential solution (see Eq. 5). Next, the velocity data is used to calculate the right hand side of the Poisson equation (Eq. 1) which was solved numerically by using the Liebmann successive over relaxation (SOR) iterative scheme (Gerald and Wheatley, 1997).

In Fig. 5. the calculated pressure result was compared with the potential pressure provided by applying the Bernoulli's equation.

$$P(x,y) = \rho U_\infty^2/2 - \rho C^2\left(x^2 + y^2\right)/2 \qquad (5)$$

U_∞^2 is the velocity in the far field (e.g. the air jet velocity) and ρ is density. A maximum relative error was found to be 0.021 when high resolution was chosen (step size was 8 pixels out of 520 pixels) and 0.082 for low resolution (step was 16 pixels).

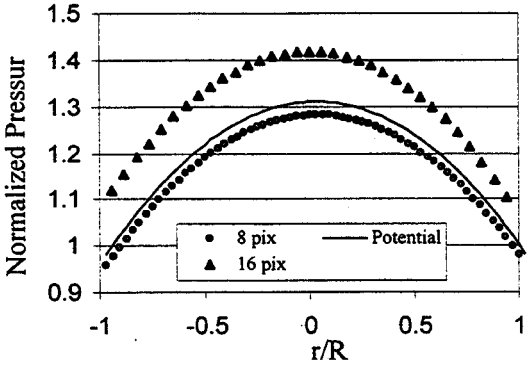

Fig. 5 A comparison between the potential solution (Eq. 5) and the numerical solution (Eq. 1) for high (8 pixels) and low (16 pixels) resolution.

The objective here was to compare pressure distribution obtained by particle image velocimetry with measured data from the literature. Peper et. al (1997) published recently results of measured pressure on a flat plate with pressure transducers for three different distances between the nozzle exit and the flat plate. Geometry and flow conditions as described in the experimental section were designed to meet the flow conditions used by Peper et al. (1997). The results in Fig. 6 were plotted using the dimensionless pressure coefficient, C_p, as a function of radial location (p is pressure, p_∞ is atmospheric pressure and V is the nozzle exit air velocity). It is shown that the pressure increases when the distance from the jet exit decreases. The pressure profiles of Fig. 6 were obtained by applying a time averaging over the instantaneous solutions of the Poisson equation (Eq. 1). Eq. 1 was solved using a Cartesian coordinate system and a Dirichlet boundary condition on three out of four boundaries (on the plate $\partial p/\partial y = 0$). In general, good agreement was found between the pressure calculation and the pressure measurements near and around the stagnation region. However, for a radial distance of $x/R_i > 1.5$, the calculated pressure deviates from the measured values. Such a deviation can be explained by the less physical use of the Dirichlet boundary condition on the sides and the choice of Cartesian formulation rather than Cylindrical. Changing the side boundary conditions from the Dirichlet type to the Neumann type will result initially in an increase of the pressure value generated by the numerical solution of the Poisson equation. However, by using cylindrical coordinate system, the value of the right hand side of the Poisson equation will become more negative (due to V_r/r) resulting in pressure reduction.

Two types of averaging could be obtained. The Poisson equation (Eq. 1) can be used to compute the instantaneous pressure for each instantaneous velocity realization and then averaged. Alternatively, the mean pressure can be calculated directly using the turbulent Poisson equation (Eq. 3) which is based on the time averaged velocity and the Reynolds stress. Fig. 7 presents a comparison between these two averaging methods.

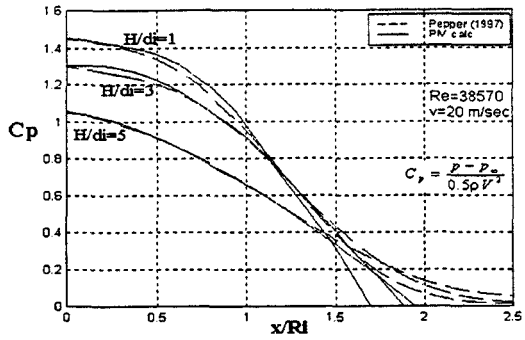

Fig. 6 The pressure distribution on the plate as calculated from the PIV velocity data and as was reported from measurements by Peper et al. (1997).

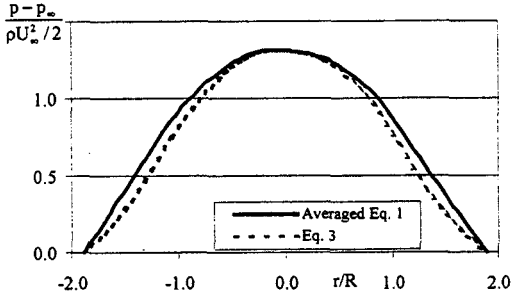

Fig. 7 A comparison between Eq. 1 and Eq. 3

As shown in Fig. 7 some deviations exist between the two averaging techniques. A possible explanation to this deviation is related to the experiment sample size. The sample size herein was 130 pair of images. Given a standard deviation of 0.1 and allowing a maximum error of 2% with 95% probability the sample size of the mean velocity at the jet center is nearly 100. The difference between the required sample size and the actual size means that the statistical error of the average velocity is somewhat smaller. However, the standard deviation of the derivative of the instantaneous velocity is larger than that of the velocity itself. When the pressure was calculated using Eq. 1, the square of the derivative of the instantaneous velocity was used to compute the right hand side, generating larger errors. On the other hand, when the mean pressure was calculated using Eq. 3, the derivative of the Reynolds stress was used. Since the standard deviation of the Reynolds stress is larger than that of the mean velocity but smaller than the standard deviation of the derivative of the instantaneous velocity we conclude that Eq. 3 generates a more accurate average pressure result.

4 Conclusions

Pressure can be obtained when spatial velocity data generated by particle image velocimetry is available. The methodology consists of two steps. The first step generates the Neumann boundary conditions by solving inversely the Navier Stokes equations. The second is a numerical solution of the pressure Poisson equation. Although velocity gradients are often noisy, the pressure assessment is usually successful because of the smoothing nature of the Poisson equation. However, PIV data must be accurate and relatively simple. Spatial resolution must be treated with special care and averaging is be handled to reduce errors.

References

Corcos GM (1963) The structure of the turbulent pressure field in boundary-layer flows, Journal of Fluid Mechanics, 18: 353-378.

Gerald CF; Wheatley PO (1997) Applied Numerical Analysis, Sixth Edition, Addison-Wesley.

Echols WH; Young JA (1963) Studies of portable air-operated aerosol generators, NRL Report 5929.

Gresho PM; Sani RL (1987) On Pressure Boundary Conditions for the Incompressible Navier-Stokes Equations, Int. J. for Numerical Methods in Fluids 7: 1111-1145.

Peper F; Leiner W; Fiebig M (1997) Impinging radial and inline jets: a comparison with regard to heat transfer, wall pressure distribution and pressure loss, Experimental Thermal and Fluid Science 14: 194-204.